EUROFUSION WPJET1-CP(16) 16563

B Grierson et al.

Validation of Theoretical Models of Intrinsic Torque in DIII-D and Projection to ITER by Dimensionless Scaling

Preprint of Paper to be submitted for publication in
Proceedings of 26th IAEA Fusion Energy Conference

This work has been carried out within the framework of the EUROfusion Consortium and has received funding from the Euratom research and training programme 2014-2018 under grant agreement No 633053. The views and opinions expressed herein do not necessarily reflect those of the European Commission.

Validation of Theoretical Models of Intrinsic Torque in DIII-D and Projection to ITER by Dimensionless Scaling

B.A. Grierson[1], C. Chrystal[2], J.A. Boedo[3], W.X. Wang[1], J.S. deGrassie[2], W.M. Solomon[2], G.M. Staebler[2], D.J. Battaglia[1], T. Tala[4], A. Salmi[4], S-P. Pehkonen[4], J. Ferreira[5], C. Giroud[6] and and JET Contributors[7]

[1]Princeton Plasma Physics Laboratory, Princeton University, Princeton, NJ 08543, USA
[2]General Atomics, P.O. Box 85608, San Diego, CA 92186-5608, USA
[3]Center for Energy Research, University of California-San Diego, La Jolla, California 92093, USA
[4]VTT, P.O. Box 1000, FIN-02044 VTT, Finland
[5]IST, Instituto de Plasmas e Fusao Nuclear, 1049-001 Lisbon, Portugal
[6]CCFE, Culham Science Centre, Abingdon, OX14 3DB, UK
[7]See the author list of Overview of the JET results in support to ITER by X. Litaudon et al. to be published in Nuclear Fusion Special issue: overview and summary reports from the 26th Fusion Energy Conference (Kyoto, Japan, 17-22 October 2016)

Corresponding Author: bgriers@pppl.gov

Abstract:
Plasma rotation experiments in DIII-D have revealed turbulent residual stress driving main-ion intrinsic rotation and used dimensionless parameter scans to predict an intrinsic torque exceeding the maximum NBI torque in ITER. In the core of low-torque dominantly electron heated plasmas with $T_e \approx T_i$, the main-ion intrinsic toroidal rotation is measured to undergo a reversal. Above a critical ECH heating power the core rotation reversal correlates with a/L_{Ti} crossing the critical gradient for ITG turbulence. Residual stress produces a counter-current intrinsic torque, which is balanced by momentum diffusion, creating the hollow profile. Quantitative agreement is obtained for the first time between the measured main-ion toroidal rotation and the rotation profile predicted by nonlinear GTS gyrokinetic simulations. In dimensionless scaling experiments that vary only ρ^*, the total intrinsic torque in the plasma is found to scale in a favorable way to ITER, projecting to increased intrinsic torque at lower ρ^*. The intrinsic torque projection for the high current H- mode phase of ITER is approximately 45 Nm, which exceeds the available neutral beam torque of 33 Nm. The combined NBI and intrinsic torque is expected to drive a modest average rotation of approximately 12 krad/s. The overall magnitude of the rotation profile and angular momentum is dependent on the boundary condition near the separatrix, and in the edge of plasmas with high and low collisionality and either sign of plasma current main-ion intrinsic rotation measurements are consistent with an orbit-loss model. Edge plasma rotation increases as collisionality decreases, projecting favorably to conditions expected in ITER.

1. Introduction

A first-principles based prediction of the rotation profile in ITER requires validated models of turbulent transport that determine the core profile shape, as well as validated models of the processes that determine the rotation boundary condition. Experiments at DIII-D are combining the validation of turbulent momentum transport in the plasma core with the intrinsic rotation at the plasma boundary to make significant advancements in our predictive capability for ITER. A series of recent experiments in DIII-D since the last IAEA FEC have advanced our understanding of intrinsic rotation by comparing the core intrinsic rotation profile to gyrokinetic simulations (Sec. 1), used dimensionally matched discharges that vary only ρ^* to determine the scaling of intrinsic torque (Sec. 2), and find a novel dependence of the edge intrinsic rotation with magnetic geometry (Sec. 3). These three contributions to a predictive understanding of intrinsic rotation are important due to the expected relatively low rotation in ITER. From the local angular momentum balance equation, validation of the transport terms (diffusion, pinch and residual stress) is

required to predict the core rotation profile. However the spatial integral of the momentum balance is required to project the total angular momentum, and includes the critical rotation boundary condition and torques in the outer region of the plasma where the gyrokinetic and gyrofluid models are not well-validated. In an axisymmetric system with vanishing core momentum flux, the boundary is where net momentum can originate and without validated models of edge momentum generation and transport more empirical projections are required.

2. Intrinsic Core Rotation Profile

Self-organized angular momentum creates an intrinsic rotation in the tokamak, where differential plasma flow can arise without direct momentum injection, and is well known to have beneficial effects on energy confinement [1] and plasma stability [2]. In ITER the rotation profile of the main-ions is expected to be influenced by intrinsic processes because the ability of auxiliary torque to drive plasma rotation will be much smaller than in existing devices, and the intrinsic rotation projections in this paper are of the same order as the neutral beam torque. ITER will operate in a regime that is dominantly electron heated by fusion alpha particles, where the heating of the ions will be dominantly through collisional energy exchange, motivating intrinsic rotation studies and model validation with direct electron heating and nearly equilibrated electron and ion temperatures.

In DIII-D we measure the main-ion (deuterium) intrinsic toroidal rotation undergoing a profile inversion, whereby an initially flat, slightly positive rotation profile reverses direction (Fig. 1) and becomes hollow. The hollow rotation profile is quantitatively predicted by global nonlinear gyrokinetic simulations. Above a critical heating power the plasma becomes linearly unstable to ion temperature gradient driven turbulence. Global nonlinear simulations with `GTS` [3] confirm a residual stress in the unstable region. Ion temperature gradient (ITG) turbulence produces a negative intrinsic torque at inner radii, driving the rotation profile in the direction opposite to the plasma current, and a positive torque at outer radii, driving the plasma in the same direction as the plasma current. The intrinsic torque is balanced by turbulent diffusion producing a local positive rotation gradient, or hollow profile, in the absence of auxiliary torque. Gyrokinetic calculations of the fluctuation-induced residual stress and resulting main-ion toroidal velocity profile that produces the zero-flux state are shown to be consistent with both the shape and magnitude of the observed rotation profile in Fig. 1.

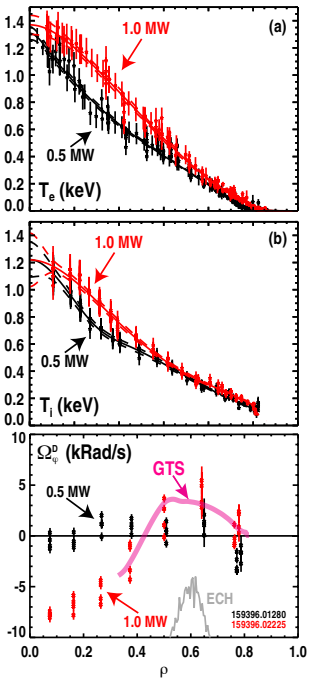

FIG. 1: Experimental temperature and rotation profiles. Rotation profile with GTS prediction of rotation profile

Core main-ion toroidal rotation reversal is obtained during an increase of direct electron heating from 0.5 to 1.0 MW. Experiments were carried out in low confinement mode (L-mode) heated by electron cyclotron waves at the second harmonic frequency positioned near the plasma half-radius. Discharges are formed with an upper-single-null shape with the magnetic field drift direction away from the active X-point and operated with $q_{95} \approx 5.5$. In these L-mode plasmas the concentration of carbon impurity is between $1.0 - 1.2\%$ such that the momentum is carried by the main-ions. Line-averaged density near $2.5 - 3 \times 10^{19}$ m^{-3} is sufficient for collisional coupling of electron and ion species such that electron cyclotron resonance heating raises both electron and ion temperatures, seen in Fig. 1(a,b), which can drive instabilities. The electron density

profile shows a small variation, and the increase of the temperature at similar density reduces the collisionality as the rotation profile hollows. Through a sequential increase in the electron heating from 0.5 to 2.2 MW in four steps (0.5, 1.0, 1.7, 2.0) we discover a reversal of the core deuterium toroidal velocity between 0.5 and 1.0 MW of applied heating, displayed in Fig. 1 for two power levels. Here the main-ion toroidal velocity profile is measured [4, 5] by short neutral beam pulses spaced approximately one second (many momentum confinement times) apart. The associated beam momentum injection on the measurement timescale is negligible. For heating powers of 1.0 MW and above the profiles are resilient to changes, the energy confinement degrades, and the the rotation profile maintains the hollow state.

Intrinsic rotation arises due to an intrinsic torque caused by turbulence in the presence of various effects that break the structure symmetry in the gyrokinetic equation [6, 7, 8], and the fluctuation symmetry in the parallel wavenumber spectrum [9, 10]. An underlying turbulent fluctuation at the ion scale in the low wavenumber range $k_\theta \rho_s \leq 1$ is required to cause momentum transport carried by the main-ions because the ion response to high-k fluctuations is nearly adiabatic. Linear turbulence stability shows that at mid-radius $\rho \approx 0.4 - 0.6$ prior to increased auxiliary heating the low-k growth rates are stable, whereas after 1.0 MW of electron heating is applied the ion temperature profile becomes linearly unstable to long-wavelength ITG modes. Displayed in Fig. 2 are the linear growth rate and frequency spectra from the `TGLF` model [11] based on measured plasma profiles including impurities, indicating that a threshold in ITG stability has been crossed by the additional heating. The lack of linearly unstable modes in Fig. 2 results in underdeveloped low-k turbulence that produces little momentum flux or residual stress. This is consistent with experimental observations that the intrinsic rotation developed in the low power phase is small.

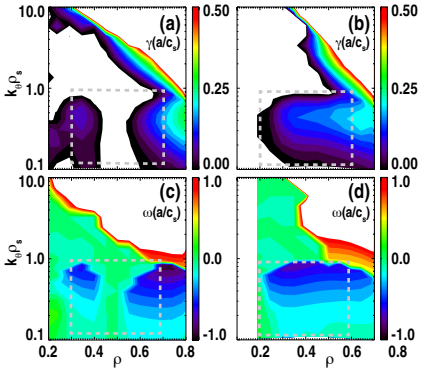

FIG. 2: TGLF linear growth rates and frequency for left:0.5 MW and right:1.0 MW

In order to compute the turbulent fluxes associated with linearly unstable ITG modes in Fig. 2(b), we use the δf global nonlinear gyrokinetic simulation `GTS` [3] with plasma profiles and equilibrium radial electric field taken directly from the experiment without adjustment. `GTS` used for this study focuses on global turbulence effects and the effect of up-down geometric asymmetry for the symmetry breaking needed for turbulence-driven toroidal momentum flux. Such global effects have been proven to be significant for turbulence to drive residual stress in many previous gyrokinetic studies. The higher order terms in the gyrokinetic equation, which are needed to break the gyrokinetic structure symmetry in the local flux-tube limit, are not included here. Simulations are electrostatic with kinetic electrons over the wavenumber range $k_\theta \rho_s \leq 2$, which covers the relevant low-k modes shown in Fig. 2.

Interpretation of plasma rotation profiles and momentum transport is guided by casting the total toroidal Reynolds stress in terms of diffusive, pinch and residual fluxes (Eq. 1), which have been studied experimentally on DIII-D [14].

$$\Pi_\varphi = -m_i n_i \langle R^2 |\nabla\rho| \rangle \left(\chi_\varphi \frac{d\Omega_\varphi}{d\rho} - V_p \Omega_\varphi \right) + \Pi^{resid.} \qquad (1)$$

where ρ denotes flux surfaces, Ω is the main-ion toroidal angular rotation frequency, χ_φ is the momentum diffusivity, V_p is the pinch velocity, $\Pi^{resid.}$ is the residual stress and the other terms are of standard usage. In steady-state the total toroidal momentum flux must be equal to zero in the absence of external toroidal torque. The balance of three terms plus the boundary condition will determine the steady state toroidal rotation profile. The residual stress component $\Pi^{resid.}$ of the total stress is directly calculated by zeroing the velocity-dependent contributions ($\Omega_\varphi = 0, d\Omega_\varphi/d\rho = 0$), and is displayed in Fig. 3. Qualitatively, the dipolar structure of the residual stress in Fig. 3 has the capability to produce a hollow intrinsic rotation profile because the associated positive intrinsic momentum flux for $\rho < 0.6$ and negative momentum flux at $\rho > 0.6$ balance against momentum diffusion. Momentum pinch is small in this case, and therefore the diffusive flux is the total flux less the residual stress.

Making an *ab initio* quantitative prediction of the intrinsic rotation requires a momentum diffusivity, pinch velocity and boundary condition. As the rotation profile itself would not available in an *ab initio* prediction to compute χ_φ, we use the the ratio of the ion momentum diffusivity to ion heat diffusivity Prandtl number $Pr \equiv \chi_\varphi/\chi_i$, whose value is well established both theoretically and experimentally to be near unity [15, 6]. The chosen Prandtl number in our model is not arbitrary, but calculated directly from the gyrokinetic simulations. The Prandtl number, on a profile average, is $Pr \approx 0.7$. This result of Prandtl number is also consistent with previous studies [16, 6]. Using the Prandtl number enables us to use $Pr\ \chi_i$ that is obtained directly from the gyrokinetic simulation, instead of χ_φ, in the prediction.

Having obtained all components of the toroidal momentum balance equation, a first-principles-based main-ion toroidal rotation profile is obtained by numerically integrating Eq. 1 for $\Omega_\varphi(\rho)$, determining the toroidal rotation profile within a constant. Displayed in Fig. 1(c) are the experimental and predicted main-ion toroidal rotation profiles during 1.0 MW ECH, where the rotation boundary conditions is taken from the experiment at $\rho = 0.8$. Good agreement between both the shape of the toroidal rotation, as well as the magnitude of the toroidal rotation variation across the profiles is accurately captured. This simulation clearly indicates that fluctuation-induced residual stress can generate intrinsic torque sufficiently strong to produce macroscopic changes in main-ion angular momentum. The level of agreement obtained represents a significant advancement in the validation of global nonlinear gyrokinetics to predict the angular momentum profiles.

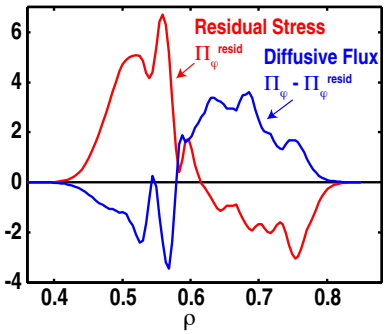

FIG. 3: Radial profile of residual stress and diffusive flux.

These experiments on DIII-D have revealed that fluctuation-induced residual stress is capable of producing the experimentally observed intrinsic main-ion toroidal rotation in both shape and magnitude. Global nonlinear gyrokinetic simulations using the experimentally measured plasma profiles predict ITG turbulence and residual stress in the radial region where the toroidal rotation undergoes a strong change of gradient. Residual stress momentum flux that arises in the gyrokinetic simulations is balanced by turbulent momentum diffusion and the turbulent momentum pinch is found to be a small contributor to the momentum transport. Integrating the momentum balance equation produces a predicted main-ion toroidal velocity profile that agrees well with the experimental measurements, demonstrating that fluctuation-induced residual stress is capable of producing experimentally observed intrinsic rotation profiles.

3. Intrinsic Torque Scaling with ρ^*

In the previous section, we have investigated the ability to predict an intrinsic rotation profile by gyrokinetic simulations. While profile predictions are required to assess the level of rotation profile shearing and tendency of the profile to peak or hollow, a prediction of the total angular momentum requires the size of the net intrinsic torque that raises the overall profile. In an effort to address how the intrinsic torque scales to ITER, a dimensionless parameter scan has been employed to determine the scaling of intrinsic torque and momentum confinement time with the normalized gyroradius ρ^*. The standard dimensionless parameter investigation methods have been used in JET, DIII-D, and ASDEX-U, so that results from all three tokamaks can be combined. The scaling with ρ^* is particularly important to investigate because the value of ρ^* for future tokamaks like ITER ($\rho^* \approx 0.002$) cannot be achieved in any current tokamaks ($\rho^* \approx 0.004$ in JET and ≈ 0.01 in DIII-D and ASDEX-U).

Figure 4 (left) shows the time history of a DIII-D discharge used to measure the intrinsic torque, and (right) profile measurements of electron density, electron temperature, ion temperature, and toroidal rotation for the high and low toroidal field discharges. The data from the low toroidal field discharges has been scaled to high field by the appropriate factors [17], and indicate a good match.

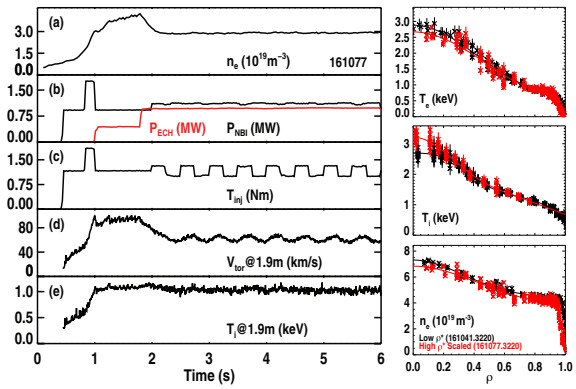

FIG. 4: (left a-e)Time history of discharge used to determine intrinsic torque. (right a-d)Plasma profiles obtained for dimensionless parameter scan varying only ρ^*

In order to measure intrinsic torque while applying torque with neutral beam injection (NBI), a 2 Hz NBI torque modulation is applied, with the basic principle of the measurement being that the relative change in the angular momentum is a result of the relative change in the applied torque. The change in the neutral beam torque can be calculated by NUBEAM, and the size of measured change relative to the total torque depends on how much intrinsic torque is present in the plasma [14]. Global momentum balance relates the rate of change of angular momentum to the total torque (NBI and intrinsic), and the angular momentum confinement time as $\dot{L} = \int(\tau_{NBI} + \tau_{int})dV - L/t_\varphi$. Here, L is the angular momentum, τ is the torque density, and t_φ is the angular momentum confinement time. A least-squares fitting routine determines what time invariant τ_{int} and t_φ generate the best match to the measured time history of the angular momentum in a discharge, given a modeled τ_{NBI}. The first fit is performed while considering the entire plasma, but subsequent fits can be done while only summing up the angular momentum and torque within a smaller minor radius in order to obtain profiles of the intrinsic torque

and momentum confinement time.

Results for intrinsic torque from the ρ^* scan are presented in Fig. 5. The total intrinsic torque contained in these plasmas was ≈ 1.5 Nm at low ρ^* and ≈ 0.7 Nm at high ρ^*. The measured values are normalized by the ion temperature (in keV) of the radius within which the measurement was made and indicated in the legend. Both have units of energy, and it is essential that the investigated parameter be normalized before any scaling with a dimensionless parameter is determined. With this normalization, the intrinsic torque is found to scale with an exponent of 1.5 ± 0.8. Based on this scaling alone, the implication is that normalized intrinsic torque will be larger in ITER than in current tokamaks.

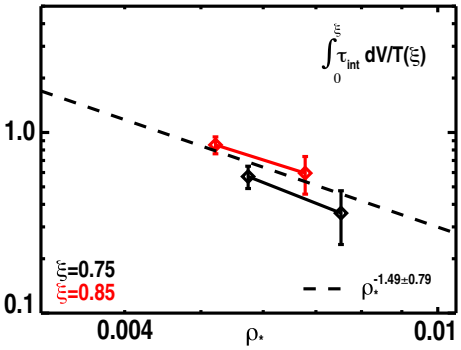

FIG. 5: DIII-D scaling of intrinsic torque with ρ^*

Through the ITPA a set of joint experiments have been carried out on JET and ASDEX for a multi-machine database of intrinsic torque scaling with ρ^* [18, 19]. Experiments were performed with low neutral beam modulation frequency of 2-3 Hz as shown in the previous section with dimensionless parameters $(\rho^*, \nu^*, \beta_N, q, T_i/T_e)$ matched between the identity shots, with good shape match between DIII-D and JET while the ASDEX shape and Mach number amongst machines could not be perfectly matched. Presented in Fig. 6 is the DIII-D and JET database normalized by ion temperature. Other normalizations with thermal stored energy and residual stress $\Pi = \rho_m, \chi_{gB} c_S$ poorly organize the data set, providing confidence that the normalization of the DIII-D data presented in the previous section is correct.

In order to project these results to ITER, the difference in ρ^* between DIII-D and ITER needs to be estimated. The density, temperature (at the top of the pedestal), toroidal field, ion mass, and minor radius in the DIII-D plasma that will be projected to ITER are 5.3×10^{19} m^{-3}, 1 keV, 3.5, 2.2 T, 2 amu, 0.55 m, respectively. This plasma is the low ρ^* plasma from the DIII-D ρ^* scan. The intrinsic torque of this plasma will be projected to an ITER plasma assumed to have the following corresponding parameters: 11×10^{19} m^{-3} (94% of Greenwald density limit at 15 MA), 5 keV (at the top of the pedestal), 3, 5.3 T, 2.5 amu (D-T mixture), 2 m. These estimations yield a ρ^* for ITER that is approximately 30% of the DIII-D values. The amount of intrinsic torque in ITER is calculated as $\tau_{ITER} = \tau_{DIII-D}(T_{ITER}/T_{DIII-D})(\rho^*_{ITER}/\rho^*_{DIII-D})^{-1.5\pm0.8}$. Using this scaling we arrive at 45 Nm of intrinsic torque, which exceeds the 33 Nm of available neutral beam torque. Taking the extrema of the uncertainty projects a range from 17-120 Nm. We can also calculate an average angular frequency by dividing the sum of the NBI and intrinsic torque by the moment of inertia and multiplying by the momentum confinement time, which is $\langle\Omega\rangle \approx 12$ krad/s. This total rotation is below the rotation frequencies obtained by uni-directional NBI in present experiments, and therefore the details of the intrinsic stresses and resulting rotation profile are of increasing importance.

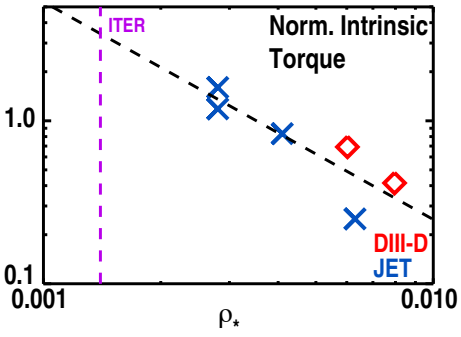

FIG. 6: Multi-machine scaling of intrinsic torque with ρ^*

4. Boundary Layer Flow and Orbit Loss

Predicting the intrinsic rotation profile and total angular momentum is made by integrating the angular momentum balance equation in space, which requires a boundary

condition. It has been commonly observed that a narrow, co-current rotation layer is observed on the outboard midplane of the tokamak maximized at the separatrix, and has also been shown that that the core plasma rotation can correlate with the separatrix flow. We have previously tested a collisionless trapped particle orbit loss model [20] including the effect of the radial electric field and found good agreement in a LSN electron cyclotron heated discharge [21]. However, recent experiments in DIII-D [22] that have inverted a single-null plasma shape from LSN to USN, have observed a reduction in the flow velocity for the USN configuration that is not captured by the model.

In the experiments we have held the magnetic field direction fixed with the ∇B drift direction down, towards the LSN primary X-point. Four discharges were executed, changing the sign of the plasma current while keeping the magnitude fixed, and inverting the plasma shape obtaining both LSN and USN configuration with mirror symmetry about the vessel midplane. The common feature observed in all four configurations is the rotation being co-current, regardless of the plasma shape. The striking difference observed is that the USN configuration with the ∇B drift direction opposite the X-point shows a strong damping of the edge flow. These results are presented in Fig. 7. The explanation for the reduction in separatrix flow in the USN configuration is due to trapped particle collisionality. Here the ion collisionality that matters for orbit loss is the ion-ion collision time normalized to the the parallel loss time (connection length / thermal speed). In the DIII-D configuration under investigation calculations of the trapped particle orbits indicate an approximate doubling of the path length for the USN shape. The effect is that the enhanced population of trapped particles in the USN configuration mitigates the loss mechanism, retaining the velocity space distribution, and avoids the generation of a net co-current plasma velocity by orbit-loss. The magnetic configuration for ITER is LSN ∇B down, which is favorable for low L-H transition power, and is also the configuration that is consistent with the maximum co-current velocity layer on DIII-D, well captured by the collisionless orbit loss model. When applying this model to ITER high current scenario using $T_{i,sep} = 50$ eV, we find a narrow velocity layer with peak velocity of 34 km/s (4.2 krad/s) with a few mm width, due to the high plasma current in ITER. By performing a temperature scan in this configuration the predicted edge velocity scales approximately linearly with T_i. The key missing ingredient to project the magnitude of the edge velocity layer to the magnitude of achieved toroidal angular momentum is a transport model that is valid in the outer region of the plasma, between the top of the pedestal and the separatrix. The relative strengths of momentum diffusion, pinch and contributions from residual stresses are all required for a comprehensive projection, and is an active area of experimental and theoretical work.

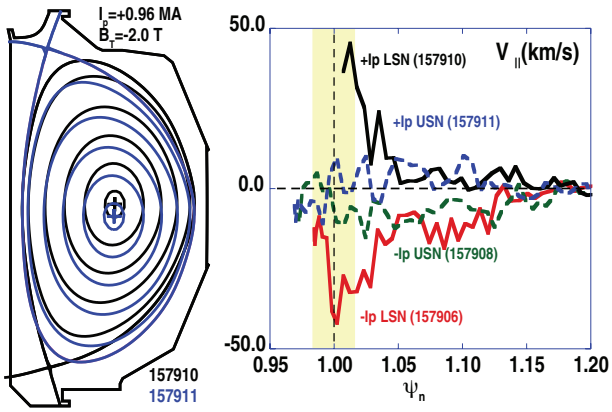

FIG. 7: Dependence on edge velocity with magnetic null

5. Conclusion

Experiments at DIII-D are combining the validation of turbulent momentum transport in the plasma core with the intrinsic rotation at the plasma boundary and have made significant advancements in our predictive capability for ITER. In the core of dominantly electron heated plasmas with $T_e \approx T_i$, the main-ion intrinsic toroidal rotation is measured

to undergo a reversal and the resulting rotation profile is accurately predicted by nonlinear gyrokinetic simulations. In the edge of plasmas with high and low collisionality and either sign of plasma current, main-ion intrinsic rotation measurements are consistent with an orbit-loss model when accounting for parallel connection. The total intrinsic torque in the plasma is found to scale favorably with ρ^* in a dimensionless scaling experiment. Due to the releatively low toroidal rotation projected by our scaling, a more detailed understanding of the self-organzed intrinsic rotation profile and shear is required to project MHD stablity and possible confinement improvement by self-generated flow shear for ITER baseline and advanced scenarios.

DIII-D data shown in this paper can be obtained in digital format by following the links at https://fusion.gat.com/global/D3D_DMP. This work supported in part by the U.S. Department of Energy under DE-AC02-09CH11466, DE-FC02-04ER54698, and DE-FG02-07ER54917

References

[1] C. L. Fiore, et. al. *Phys. Plasmas*, vol. 19, pp. 056113–056113–7, Apr. 2012.

[2] J. W. Berkery, et. al. *Physical Review Letters*, vol. 104, no. 3, p. 035003, 2010.

[3] W. X. Wang, et. al. *Phys. Plasmas*, vol. 13, no. 9, p. 092505, 2006.

[4] B. A. Grierson, et. al. *Rev. Sci. Instrum.*, vol. 83, p. 10D529, Aug. 2012.

[5] B. A. Grierson, et. al. *Phys. Plasmas*, vol. 19, pp. 056107–056107–14, Mar. 2012.

[6] A. G. Peeters, et. al. *Phys. Plasmas (1994-present)*, vol. 12, p. 072515, July 2005.

[7] F. I. Parra, et. al. *Physics of Plasmas*, vol. 18, no. 6, p. 062501, 2011.

[8] H. Sugama, et. al. *Plasma Physics and Controlled Fusion*, vol. 53, p. 024004, Jan. 2011.

[9] P. H. Diamond, et. al. *Nuclear Fusion*, vol. 49, p. 045002, Mar. 2009.

[10] F. I. Parra and M. Barnes, *Plasma Physics and Controlled Fusion*, vol. 57, p. 045002, Mar. 2015.

[11] G. M. Staebler, et. al. *Phys. Plasmas*, vol. 12, no. 10, p. 102508, 2005.

[12] R. J. Hawryluk, et. al. *Course on Physics of Plasmas Close to Thermonuclear Conditions*, pp. 1–28, 1979.

[13] W. X. Wang, et. al. *Phys. Plasmas*, vol. 17, no. 7, p. 072511, 2010.

[14] W. M. Solomon, et. al. *Nuclear Fusion*, vol. 49, p. 085505, July 2009.

[15] N. Mattor and P. H. Diamond, *Physics of Fluids*, vol. 31, no. 5, p. 1180, 1988.

[16] F. J. Casson, et. al. *Phys. Plasmas*, vol. 16, no. 9, p. 092303, 2009.

[17] C. C. Petty *Phys. Plasmas*, vol. 17, no.5, p. 056108, 2010.

[18] T. Tala, et. al. *Proceedings of European Physical Society*, O2.104, 2016.

[19] S-P. Pehkonen, et. al. *Proceedings of European Physical Society*, P2.011, 2016.

[20] J. S. deGrassie, et. al. *Nucl. Fusion* vol. 52, no. 13, p. 13010, 2012.

[21] R. J. Buttery, et. al. *Nucl. Fusion* vol. 55, no. 10, p. 104017, 2015.

[22] J. A. Bodeo, et. al. *Phys. Plasmas* vol. 23, no. 9, p. 092506, 2016.